Detection of Basal Cancer Cells using Photodetector Based on a Novel Surface Plasmon Resonance Nanostructure Employing Perovskite Layer with an Ultra High Sensitivity

Article *in* Plasmonics · October 2022

DOI: 10.1007/s11468-022-01727-3

CITATIONS
17

READS
201

9 authors, including:

Malek G. Daher
Islamic University of Gaza
64 PUBLICATIONS **419** CITATIONS
SEE PROFILE

Youssef Trabelsi
University of Tunis El Manar
60 PUBLICATIONS **581** CITATIONS
SEE PROFILE

Associate Professor Dr Naser Mahmoud Ahmed
Universiti Sains Malaysia
402 PUBLICATIONS **4,130** CITATIONS
SEE PROFILE

Vishal Sorathiya
Parul Universiy
104 PUBLICATIONS **1,633** CITATIONS
SEE PROFILE

Plasmonics
https://doi.org/10.1007/s11468-022-01727-3

Detection of Basal Cancer Cells using Photodetector Based on a Novel Surface Plasmon Resonance Nanostructure Employing Perovskite Layer with an Ultra High Sensitivity

Malek G. Daher[1,2] · Youssef Trabelsi[3,4] · Naser M. Ahmed[2] · Yogenra Kumar Prajapati[5] · Vishal Sorathiya[6] · Sk Hasane Ahammad[7] · P. Poorna Priya[8] · Osama S. Faragallah[9] · Ahmed Nabih Zaki Rashed[10]

Received: 28 June 2022 / Accepted: 17 October 2022

Abstract
Today, basal cancer cells is one of the most frequent diseases on the planet, which is global concern for human health. In order to maximize the success of treatment, early detection is a vital prerequisite. So, a rapid and sensitive detection of cancerous basal cells is a necessary topic. In this paper, a photodetector based on SPR nanostructure consisting prism (N-FK51A), silver (Ag), hybrid organic–inorganic halide perovskites (MAPbX3 ≡ CH3NH3PbY3, with M = CH3, A = NH3 and Y = Br), and graphene layers is suggested theoretically for the detection of cancerous basal cells. It is demonstrated that the proposed photodetector with perovskite has a superior efficiency than the conventional without perovskite. Silver, perovskite, and graphene layers of suggested SPR nanostructure have been optimized to achieve the highest efficiency. The highest reached sensitivity is 298.5 deg/RIU with the optimal thicknesses of Ag (60 nm), $MAPbBr_3$ (3 nm), and the optimal number of graphene layers is equal to three layers. This sensitivity is ultra-high value compared to latest work that utilizes SPR configuration. As a result, the proposed SPR photodetector nominates as a strong candidate for use in several areas of biosensing applications.

Keywords Basal cancer · Surface plasmon · Transfer matrix · Perovskite · Sensitivity

Introduction

Due to their distinct features such as ability to perform real-time detection in a label-free platform, high sensitivity, and quick response, the surface plasmon resonance nanostructure is utilized in a lot of chemical and biosensing applications such food safety, medical diagnostics, and drug diagnostics [1–4]. The metals that can support plasmons in SPR sensors are silver, gold, indium, aluminum, copper, and sodium. Silver can be used if its oxidation can be minimized by coating another layer above it [5]. Due of the strong plasmonics interaction with incident light, it has drawn attention from the scientific community on a global scale [6]. The basis of an SPR photo-detector is to decide the change in the RI of an analyte when bio-molecules interact on the SPR structure surface. The SPR condition can be determined by phase matching of the evanescent wave generated by the transverse magnetic (TM) light and wave of surface plasmon (SP). A dip is produced in the reflectance spectrum when the SPR condition is accomplished. The employed prism, incident light wavelength, 2D materials, metals, and biomolecule binding are some factors that affect the angle of the reflectance dip [7]. The reflectance profile can be used to decide the sensing performance of the SPR photo-detector.

Two-dimensional nanomaterials such as black phosphorus (BP), graphene (G), and transition-metal dichalcogenides (TMDGs) have a lot of interest in SPR sensors because of their distinct optical and electrical properties [7]. Chemical vapor deposition is a method that can be utilized to create 2D nanomaterials [8]. To obtain desired electrical characteristics for improved biosensing, the number of 2D nanomaterial layers can be adjusted. Recently, graphene has become a new possibility for enhancing the sensitivity of various kinds of optical sensors. It has been demonstrated that adding a graphene monolayer over a metal increases the sensitivity of the detector [9]. Researchers from all over the world have been drawn to graphene because of its highly

✉ Ahmed Nabih Zaki Rashed
ahmed_733@yahoo.com

Extended author information available on the last page of the article

Published online: 27 October 2022

intriguing mechanical, electrical, and optical properties. The lowest resistivity, lowest bandgap, and high electron mobility are among these characteristics [10, 11]. It is also a much better biomolecule adsorbent than metals due to its high surface to volume ratio. Because of its carbon-based atomic ring structure, graphene has a high capacity for biomolecule adsorption. This is due to π stacking interaction between its hexagonal cells and the common carbon-based ring constructions seen in biomolecules [12]. Consequently, graphene is a superior substance for biomolecule adsorption and can thus greatly increase the efficiency of the SPR photodetectors. Hybrid organic–inorganic halide perovskites have seen a surge in research attention recently as inexpensive solution-processed materials with interesting applications [13, 14]. As a result, they can be found in light emitting diodes (LED) [15], photodetectors [16], photovoltaics [17], and nanowire lasers [18]. Additionally, the expression for organic–inorganic perovskites is CH3NH3PbX3 (MAPbY3), where Y is either Br, Cl, or I [19, 20]. MAPbY3 can be seen as a novel plasmonic material and a strong contender for sensing applications throughout the entire visible spectrum. This is because of their exceptional stability, minimal band gap, and great optical absorption, which have all led to their exhibiting exceptional optical and electrical properties [21, 22].

Human health is dangerously compromised by the basal cancer cells [23]. One form of skin cancer is basal cell carcinoma. Though it can take numerous modes, it frequently manifests as a small, slightly translucent lump on the skin. Cancerous basal cell most commonly appears on skin that is exposed to the sun, such as your head and neck [24, 25]. The body could become infected with cancer and ultimately kill the patient if the injured cells are not discovered at an early stage. [26]. There are numerous ways to find malignant cells, including electrochemical techniques [27], immunocytochemistry [28], and microfluidic devices [29]. Since these devices are expensive and need for sophisticated equipment, it is necessary to identify malignant cells with accuracy and reality utilizing quick, inexpensive methods. In this work, we suggest an SPR-based photodetector that uses a thin layer hybrid organic–inorganic halide perovskites on the top of a silver and two-dimensional graphene layer is inserted between the sensing medium and the perovskites thin film. We rely on the doctor to be designed at room temperature. The sensing capabilities of the photo-detector are examined using the transfer matrix technique (TMM). The proposed SPR nanostructure's layer thicknesses have been optimized to achieve higher sensitivity.

Structure Consideration and Theoretical Model

The suggested detector has five layers N-FK51A prism, silver, perovskite, graphene, and sensing layer for the detection of basal cancer cells. The thicknesses of silver, perovskite, and graphene layers are signified as h_2, h_3, and h_4 and the refractive indices are indicated as n_2, n_3, and n_4, respectively. A suggested SPR biosensor based on layers of Ag, perovskite, and graphene is shown schematically in Fig. 1.

The following relationship that describes the dispersion of refractive index of the glass prism (N-FK51A) can be obtained as [30]:

$$n(\lambda) = \left(1 + \frac{s_1\lambda^2}{\lambda^2 - r_1} + \frac{s_2\lambda^2}{\lambda^2 - r_2} + \frac{s_3\lambda^2}{\lambda^2 - r_3}\right)^{0.5} \quad (1)$$

where s_1, s_2, s_3, r_1, r_1, and r_3 are the Sellmeier coefficients. The value of these coefficients are as $r_1 = 0.00472301995$, $r_2 = 0.0153575612$, $r_3 = 168.68133$, $s_1 = 0.971247817$,

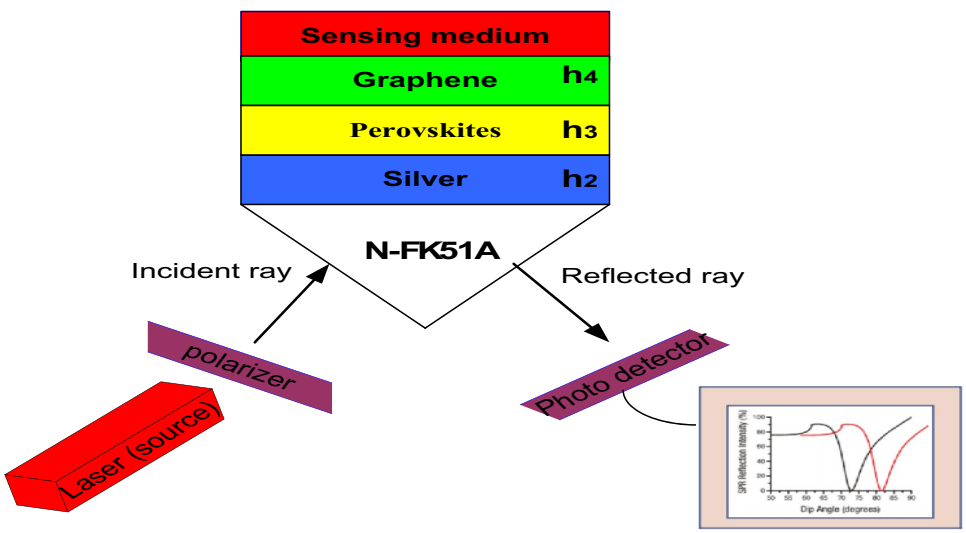

Fig. 1 A schematic representation of an SPR photodetector employing perovskite layer

Table 1 The used layers and their refractive indices at $\lambda = 632.8$ nm

The used layer	Refractive index (RI)	Ref.
MAPBr3 (perovskite)	2.008 + 0.0013i	[32]
Graphene	3 + 1.149106i	[33]

$s_2 = 0.216901417$, and $s_3 = 0.904651666$. λ is the incident light's wavelength in μm. The index of the Ag layer dependents on the incident light wavelength and is obtained by Drude–Lorentz model [31]

$$n_{Ag}(\lambda) = \left(1 - \frac{\lambda_c \lambda^2}{\lambda_p{}^2 (\lambda_c + i\lambda)}\right)^{1/2} \tag{2}$$

where the collision and plasma wavelengths of Ag are $\lambda_c = 1.7614 \times 10^{-5} m$ and $\lambda_p = 1.4541 \times 10^{-7} m$, respectively. The refractive indices of perovskite ($MAPBr_3$) and graphene are presented in Table 1.

The reflectivity of the structure has been calculated using the transfer matrix approach for the L-layer system. This technique is efficient since it does not associate with any approximations. Along the z-axis, all of the layers are organized into a stack. The thickness and dielectric constant for each layer are d_k and ε_k respectively. The tangential fields at the first border ($z = 0$) and the final border are connected ($z = z_{L-1}$), mathematically [34]:

$$\begin{bmatrix} A_1 \\ B_1 \end{bmatrix} = W \begin{bmatrix} A_{L-1} \\ B_{L-1} \end{bmatrix} \tag{3}$$

where the tangential electric fields at the boundaries of the first layer and the Lth layer are A_1 and A_{L-1}, respectively. The tangential magnetic fields at the first layer boundary and the Nth layer boundary are B_1 and B_{N-1}, respectively. For j-layer, the specific matrix (W_j) is obtained by [34, 35]:

$$W_j = \begin{bmatrix} \cos(\beta_j) & -\frac{i \sin(\beta_j)}{X_j} \\ -i X_j \sin(\beta_j) & \cos(\beta_j) \end{bmatrix} \tag{4}$$

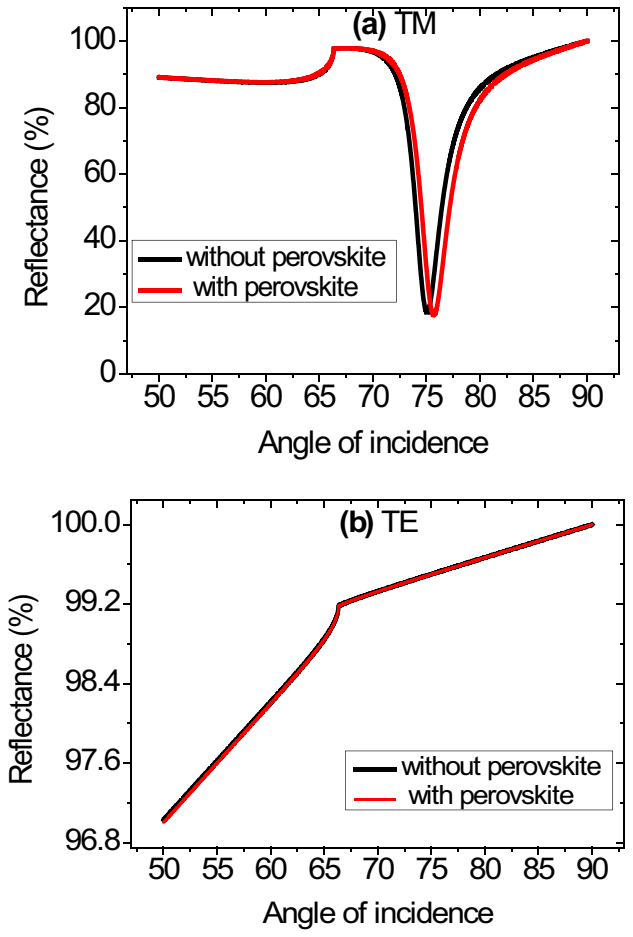

Fig. 2 Reflectance spectra for the suggested SPR photodetector at $n_{SM} = 1.36$ for TM and TE polarizations

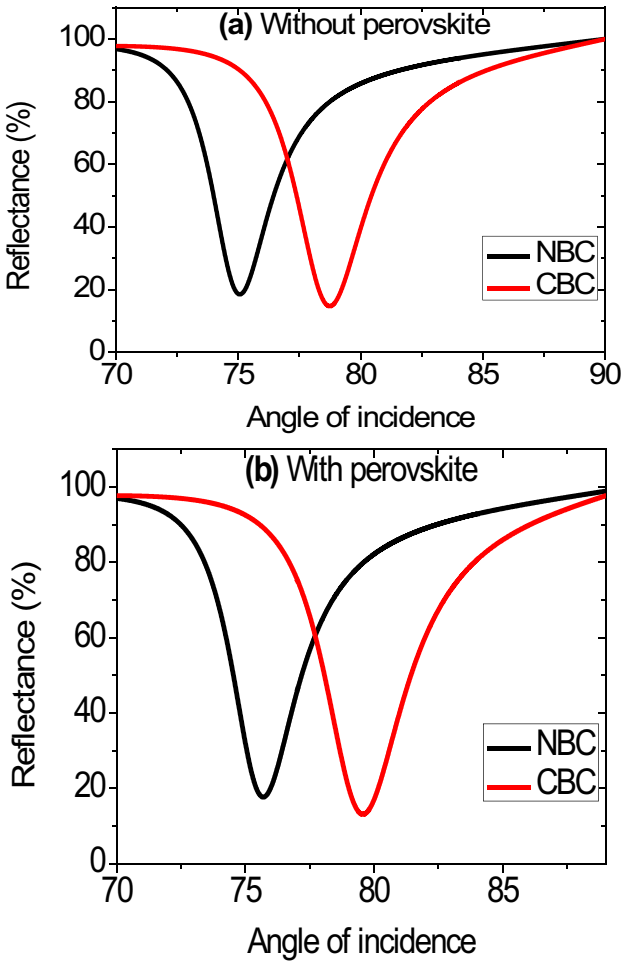

Fig. 3 Reflectance curves of the suggested SPR sensors. **a** Without perovskite layer and **b** with perovskite layer at $h_2 = 40$ nm, $h_3 = 1$ nm, and $h_4 = N \times 0.34$ nm where $N = 1$

Table 2 The used structures and their sensitivity at $h_2 = 40$ nm, $h_3 = 1$ nm, and $h_4 = N \times 0.34$ nm where $N = 1$

The used structure	Cell	RI	θ_{Res}(deg)	$\Delta\theta_{Res}$(deg)	S (deg/RIU)
Without perovskite layer	NBC	1.36	75.09	-	-
	CBC	1.38	78.72	3.63	181.5
With perovskite layer	NBC	1.36	75.69	-	-
	CBC	1.38	79.58	3.89	194.5

β_j is the light wave's phase variation as it passes through the j[th] layer.

$$\beta_j = \frac{2\pi}{\lambda} h_j (\varepsilon_j - (n_1 \sin\ \theta_1)^2)^{1/2} \tag{5}$$

where hj and εj are the jth layer's thickness and dielectric constant, respectively. The incident light's wavelength, incidence angle, and refractive index of prism are represented as $\lambda, \theta_1,\ and\ n_1$.

$X_j = (\varepsilon_j - (n_1 \sin\ \theta_1)^2)^{0.5} / \varepsilon_j$ for p-polarized light. The full characteristic matrix S of the structure can be expressed as:

$$S = W_{Ag} W_P W_G = \begin{bmatrix} S_{11} & S_{12} \\ S_{21} & S_{22} \end{bmatrix} \tag{6}$$

where W_{Ag}, W_P, and W_G are the characteristic matrices of the metal, provskite, and graphene layers, respectively. The intensity of reflectance (R) of TM waves for L-layer structure can be obtained as [35]:

$$R = \left| \frac{(S_{11} + S_{12}X_N)X_1 - (S_{21} + S_{22}X_N)}{(S_{11} + S_{12}X_N)X_1 + (S_{21} + S_{22}X_N)} \right|^2 \tag{7}$$

Results and Discussion

An SPR structure-based photodetector is explored for the detection of basal cancer cells. According to the previous section, the refractive indices of the layers are determined at $\lambda = 632.8$ nm. The thicknesses are chosen as $h_2 = 40$ nm, $h_3 = 1$ nm, and $h_3 = N \times 0.34$ nm where $N = 1$ for metal (Ag), perovskite ($MAPbBr_3$), and graphene layers, respectively. The prism used as the substrate. In the case of a prism-based SPR sensor, it is known that the evanescent wave required to excite surface plasmons results from the prism-metal interface's total internal reflection when the angle of incidence of the beam is greater than the critical angle. The prism assists in coupling the horizontal wave vector components of the incident light to the propagating wave vector of surface plasmon polaritons (SPP) [36, 37]. Generally, the thickness of the prism is considered semi-infinite (approximately 1.5 to 2.5 cm). If the thickness of the prism is larger, then there might be more scattering loss. The group of authors used the thickness of a prism of 2.5 cm for DNA hybridization [38].

We begin by demonstrating the proposed SPR nanostructure's polarization-dependent optical response using reflectance spectra. Figure 2 exhibits the reflectance spectrum of the proposed detector for transverse-magnetic (TM) polarization which is demonstrated in Fig. 2a while for transverse-electric (TE) polarization, it is presented in Fig. 2b. It can be observed that the reflectance curve for TE mode is almost fat while the surface plasmon resonance phenomenon (SPR) occurs in the TM mode through resonant dips that appear in the spectrum. As a result, the surface plasmon (SP) can be excited only as the incident wave has TM polarization.

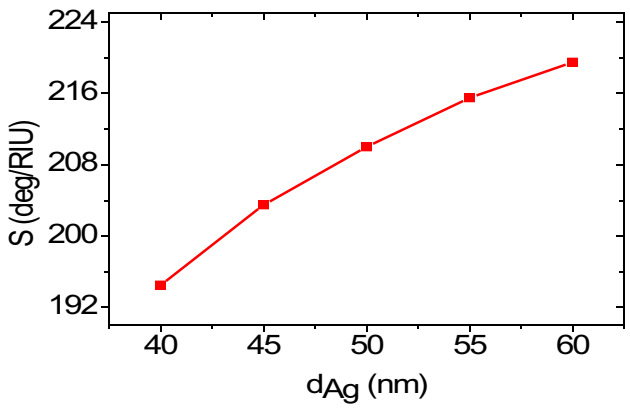

Fig. 4 Sensitivity versus thickness of the metal (Ag) at $h_3 = 1$ nm and $h_4 = N \times 0.34$ nm where $N = 1$

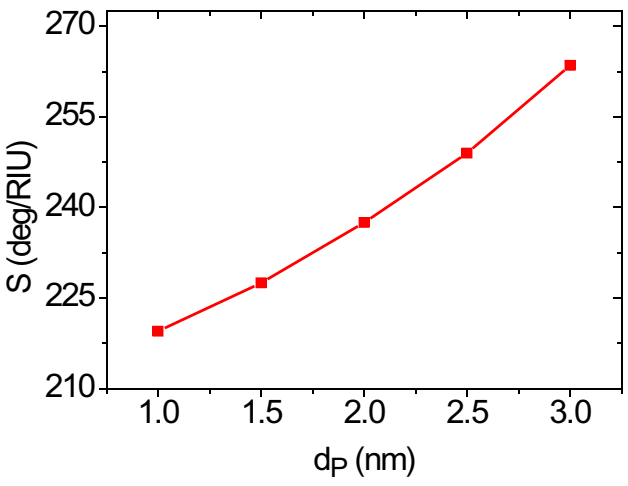

Fig. 5 Sensitivity versus thickness of perovskite at $h_2 = 60$ nm and $h_4 = N \times 0.34$ nm where $N = 1$

Table 3 Variation the sensitivity with different thicknesses of Ag at $h_3 = 1$ nm and $h_4 = N \times 0.34$ nm where $N = 1$

Thickness of Ag (nm)	Position of resonant dip of NBC θ_{Res1} (deg)	Position of resonant dip of CBC θ_{Res2} (deg)	$\Delta\theta_{Res}$ (deg)	S (deg/RIU)
40	75.69	79.58	3.89	194.5
45	75.83	79.9	4.07	203.5
50	75.92	80.12	4.2	210
55	75.99	80.3	4.31	215.5
60	76.03	80.42	4.39	219.5

Thus, the TM-polarized light's evanescent field permeates the metal layer and may excite the SP waves that are traveling along the metal film surface [39, 40]. Hence, the complete amount of the TM-polarized incident wave energy is transformed to SP at resonance condition [41]. For that reason, the SPR photodetectors can only use incident light that is TM-polarized. Figure 3a, b depict the SPR reflectivity spectra for both normal and cancer basal cells (NBC and CBC) as sensing media. The shift of the dip in the reflectance spectrum of TM light serves as the basis for the detecting mechanism of the proposed biosensor. The difference in refractive index between healthy cells and cancer cells causes this shift [23, 26]. Figure 3a gives the reflectance spectra of the proposed sensor with a perovskite layer thickness of 0 nm while the reflectance spectra in Fig. 3b with a perovskite layer thickness of 1 nm (MAPbBr3). As the analyte's refractive index rises, it can be seen that the minimum reflectance corresponding to the resonance angle lightly decreases. As the refractive index of the analyte increases, a second aspect is that the resonance angle of dip transfers to a higher angle. It is observed that resonance angles of dips swing from 75.09 to 78.72 and 75.69 to 79.58 for SPR structure without the $MAPbBr_3$ layer and SPR structure with 1 nm of MAPbBr3 layer, respectively. Thus, introducing of 1 nm MAPbBr3 layer improves the sensitivity by at least 7% for SPR sensor based on perovskite as shown in Table 2. The performance of SPR sensor also depends on the field distribution of SPs at metal–dielectric interface. It is well known that the electromagnetic (EM) field of SP peaks at the metal-sensing layer interface and decays exponentially within only a fraction of a wavelength which is termed as evanescent field. The plot of TM field normal to different interfaces of constituent layers of the proposed SPR sensor shows the field distribution at different layer interfaces. Generally, it rises with metal thickness, becomes maximum at 2D nanomaterial interface, and then it exponentially decreases in sensing medium. The maximum field at 2D nanomaterial interface is due to strong control, manipulation, and confinement of charge carriers on using 2D nanomaterial or their heterostructures. The depth of the TM field may be analyzed by evaluating penetration depth (PD). PD indicates the interaction length of SPs in sensing medium at which TM field decays by 37% of its maximum value. Larger PD is suitable for deep analyte sensing by increasing the interaction volume with the biomolecules present in the sensing medium [42]. Mathematically, the interaction is represented by an overlap integral between the evanescent field of SPs and spatial distribution of dielectric constant of the sensing region in three-dimensional space. Depending upon the interactions, the overlap integrals are different and accordingly, the reflectivity spectra are different. Hence, the reflectivity is proportional to the overlap volume and accordingly, the sensitivity of thin film-based SPR sensor is proportional to overlap integral. Therefore, sensitivity of proposed configuration can be enhanced by increasing the overlap integral in the overlap volume. One can achieve this by increasing the field's peak height at metal-sensing layer interface and its penetration depth into the sensing region [43].

A suitable option of the layers thicknesses of the structure is required to get the best sensitivity of the SPR sensor. As a result, various options and optimization processes for the layers thicknesses of the structure will be investigated and studied. In the first, we methodically study the influence of the thickness of metal layer on the sensitivity. The thickness of perovskite and graphene layers has been fixed as $h_3 = 1$ nm (for perovskite) and $h_4 = L \times 0.34$ nm where $L = 1$ (for graphene). Figure 4 exhibits the change

Table 4 Variation the sensitivity with different thicknesses of perovskite at $h_2 = 60$ nm and $h_4 = N \times 0.34$ nm where $N = 1$

Thickness of perovskite (nm)	Position of resonant dip of NBC θ_{Res1} (deg)	Position of resonant dip of CBC θ_{Res2} (deg)	$\Delta\theta_{Res}$(deg/RIU)	S (deg/RIU)
1	76.03	80.42	4.39	219.5
1.5	76.41	80.96	4.55	227.5
2	76.79	81.54	4.75	237.5
2.5	77.2	82.18	4.98	249
3	77.62	82.89	5.27	263.5

Table 5 Variation the sensitivity with different number of graphene layer at $h_2 = 60$ nm and $h_3 = 3$ nm

Number of graphene layers	Position of resonant dip at NBC θ_{Res1} (deg)	Position of resonant dip at CBC θ_{Res2} (deg)	$\Delta\theta_{Res}$(deg/RIU)	S (deg/RIU)
1	77.62	82.89	5.27	263.5
2	78.17	83.78	5.61	280.5
3	78.73	84.7	5.97	298.5
4	79.39	85.2	5.84	292

of sensitivity with increasing thicknesses the silver layer. As the thickness of the Ag layer rises from 40 to 60 nm, it can be seen that the sensitivity climbs from 194.5 to 219.5 deg/RIU. Consequently, we can say that the sensitivity is regularly enhanced with increasing the thickness of silver layer reaching its maximum at h2 = 60 nm. Surface plasmons (SPs) gain the ability to transfer incident light energy to them as the thickness of the metal layer grown. As a result, a strong excitation of SP follows and leads to sensitivity and quality enhancement of the biosensor. For $h_2 > 60$ nm, the resonant dip vanishes. As a result, 60 nm is chosen as the optimal Ag layer thickness for the greatest performance of the suggested SPR photodetector. Therefore, it is observed that $h_2 = 60$ nm will be considered in the next investigations. The calculations of dip positions, shift of resonant angle, and sensitivity for all those thicknesses of Ag layer are presented in Table 3.

Furthermore, to determine the impact of perovskite layer thickness on the effectiveness of the suggested photodetector, we have studied the sensitivity of the proposed SPR detector for different values of thickness of the perovskite layer. Here, the perovskite layer's thickness has been adjusted in steps of 0.5 nm from $h_3 = 1$ to $h_3 = 3$ nm. The thicknesses: $h_2 = 60$ nm and $h_4 = N \times 0.34$ nm where $N = 1$ for the SPR nanostructure is fixed. It can be observed that the sensitivity gradually improves with increasing the thickness of perovskite ($MAPbBr_3$). The sensitivity of proposed SPR photodetector with varying thickness of perovskite ($MAPbBr_3$) layer is plotted in Fig. 5. The top sensitivity of suggested SPR photodetector is 263.5 deg/RIU as the thickness of perovskite is 3 nm. Consequently, we will consider the thickness of perovskite ($h_3 = 3$ nm) in the following discussion. The calculations of position of dips, angle shift, and sensitivity of the suggested SPR detector are presented in Table 4.

Now, to determine the optimal amount of graphene layers which obtain the highest sensitivity of the suggested SPR photodetector, we have examined the efficiency of the suggested photodetector with growing the number of the graphene layer as presented in Table 5. As a result, the SPR nanostructure is fixed by the following parameters: $h_2 = 60$ nm and $h_3 = 3$ nm for metal (Ag) layer and perovskite ($MAPbBr_3$) layer, respectively. It is important to note that the sensitivity increases with the addition of more graphene layers ($N = 1$ to 3) and then drops for $N > 3$. Thus, the optimal number of graphene layer can be selected as $N = 3$ for the suggested SPR photodetector. Figure 6 exhibits the fluctuation of sensitivity with increasing the number of graphene layer. Based on above investigation, the best performance of the suggested SPR photodetector can be achieved as the nanostructure of SPR photodetector is characterized by the optimized thicknesses: $h_2 = 60$ n, $h_3 = 3$ nm, and $h_4 = N \times$

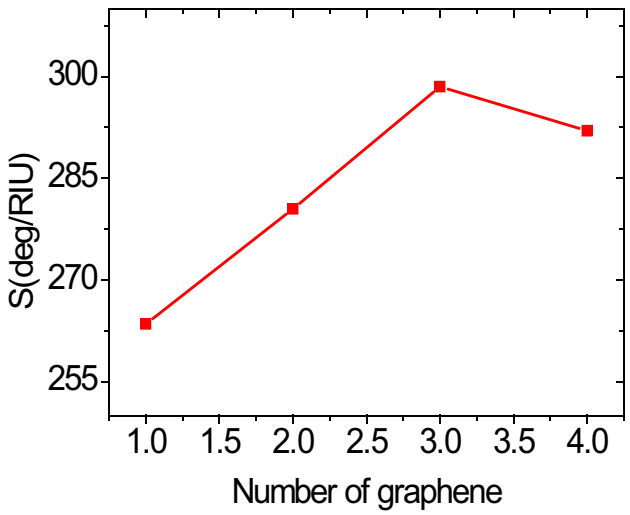

Fig. 6 Sensitivity of the proposed SPR photodetector versus number of graphene layer at $h_2 = 60$ nm and $h_3 = 3$ nm

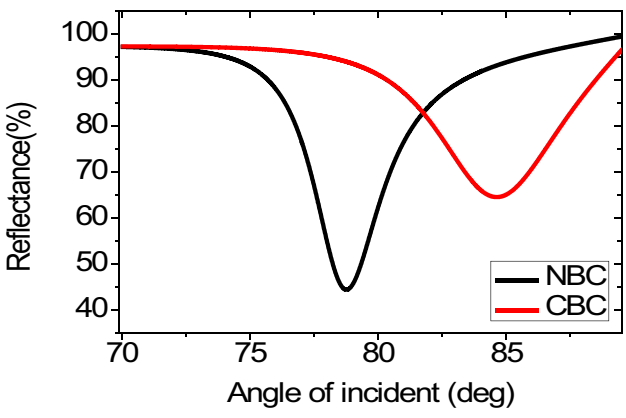

Fig. 7 Reflectance curves of the suggested SPR photodetector with perovskite layer at $h_2 = 60$ nm, $h_3 = 3$ nm, and $h_4 = N \times 0.34$ nm where $N = 3$

Table 6 Comparing the sensitivity of this research to the most recent SPR-based biosensors that have been published

Techniques/structures	Year	Sensitivity (deg/RIU)	Reference
SPR detector employing a thin layer of graphene	2018	121.7	[44]
SPR detector using MXene and black phosphorus	2019	190.22	[45]
ZnO-based SPR photodetector for DNA hybridization	2020	157	[46]
SPR photodetector employing plasma layer	2021	102.9	[47]
Sensing of the bacteria using SPR biosensor based on graphene sheets	2022	199.87	[30]
SPR biosensor based on titanium disilicide and black phosphorus	2022	195.4	[48]
SPR biosensor based on graphene as a 2D-nanomaterial	2022	161	[49]
SPR photo-detector employing perovskite layer for the detection of basal cancer cells	**2022**	**298.5**	**Current work**

0.34 nm where $N = 3$ for metal (Ag), perovskite ($MAPbBr_3$, and graphene layers, respectively. The reflectance intensity corresponding the angle of incident at those optimized conditions is shown in Fig. 7. The sensitivity is obtained as 298.5 deg/RIU at optimum conditions. The full width at half maximum (FWHM) is 4.05 deg. As a result, the detection accuracy (DA) is calculated and obtained as 0.246 deg^{-1} according the following equation: DA = 1/FWHM. Finally, the figure of merit is computed and found as 73.43 RIU^{-1} according the following relation: FOM = S × DA.

It is clear that an excellent sensitivity of 298.5 deg/RIU is obtained in the proposed SPR photodetector which is not achieve in the recently reported sensors. Table 6 also provides a comparison of the proposed and recently reported works in tabular format. Furthermore, the suggested photodetector has a simple structure to fabricate, quick real-time detection, tunable design, and low cost. With these wonderful advantages, we think that the suggested SPR photodetector, which is based on a perovskite (MAPbBr3) layer, can be extensively applied in the field of bio-sensing applications. As a result, it can be employed for the detection of basal cancer cells and any biological analyte.

Giving some advice about how to fabricate the proposed sensor is really important. On the top of the BK7 prism, a thin film of Ag (60 nm) is placed. Deposition techniques such vacuum thermal evaporation, electron beam evaporation, ion plating evaporation, and laser beam evaporation are frequently used. Perovskite is grown as a 3 nm-thin layer on the silver film. Useful deposition techniques include the following: photo CVD, thermal CVD, HOMO (hot reactor and cold substrate) CVD, and thermal CVD for a perovskite film. Then, using CVD or electrospinning methods, thin graphene sheets are deposited on the perovskite coating.

Conclusion

An SPR-based photodetector based on perovskite (MAPBBr3) has been designed for the detection of cancerous basal cells. We analyzed the reflectance of the suggested photodetector using the transfer matrix approach (TMM). Silver (Ag), hybrid organic–inorganic halide perovskites, and graphene layers of suggested SPR have been investigated for the best performance. We first examined the sensor performance for the structures: prism of N-FK51A glass/silver/graphene/analyte (structure 1) and prism of N-FK51A glass/silver/perovskite/graphene/analyte (structure 2) and found that structure 2 has the highest sensitivity of 194.5 deg./RIU with 7% improvement over structure 1. Also, it is found that the sensitivity enhances with rising the thickness of Ag and $MAPbBr_3$ layers. On the other hand, it is found that the sensitivity improves with the growing number of graphene layers until three layers and then drops. A highest sensitivity of 298.5 deg./RIU is reached with silver (60 nm), perovskite (3 nm), and a triple layer of graphene. This structure will be recommended for fabricating new sensing devices in the field of cancerous basal cells sensing. Also, it is expected that the proposed photodetector is noble for the detection of other cancer cells and biomolecules with high efficiency. Finally, we recommend to do this proposed SPR structure experimentally in future research.

Author Contribution Conceptualization: Malek G. Daher and Naser M. Ahmed. Data curation, formal analysis, and investigation: Malek G. Daher, Y. K. Prajapati, and Vishal Sorathiya. Methodology: Sk Hasane Ahammad, P. Poorna Priya, and Ahmed Nabih Zaki Rashed. Resources and software: Malek G. Daher, Youssef Trabelsi, and Naser M. Ahmed. Supervision and validation: Sk Hasane Ahammad, P. Poorna Priya, Osama S. Faragallah, and Ahmed Nabih Zaki Rashed. Visualization and writing — original draft: Malek G. Daher, Youssef Trabelsi, Y. K. Prajapati, Vishal Sorathiya, and Ahmed Nabih Zaki Rashed.

Funding This research was supported by the Deanship of Scientific Research- Research Center at King Khalid University in Saudi Arabia for funding this research (code number: RGP 2 /23/43).

Availability of Data and Material Simulation software.

Code Availability Not applicable.

Declarations

Ethics Approval Not applicable.

Consent to Participate Not applicable.

Consent for Publication Not applicable.

Conflict of Interest The authors declare no competing interests.

References

1. Almawgani AH, Taya SA, Daher MG, Colak I, Wu F, Patel SK (2022) Detection of glucose concentration using a surface plasmon resonance biosensor based on barium titanate layers and molybdenum disulphide sheets. Physica Scripta 97:065501
2. Pal A, Jha A (2021) A theoretical analysis on sensitivity improvement of an SPR refractive index sensor with graphene and barium titanate nanosheets. Optik 231:166378
3. Karki B, Ramya KC, Sandhya Devi RS et al (2022) Titanium dioxide, black phosphorus and bimetallic layer-based surface plasmon biosensor for formalin detection: numerical analysis. Opt Quant Electron 54:451. https://doi.org/10.1007/s11082-022-03875-6
4. Yupapin P, Trabelsi Y, Vigneswaran D, Taya SA, Daher MG, Colak I (2021) Ultra-high sensitive sensor based on surface plasmon resonance structure having Si and graphene layers for the detection of chikungunya virus. Plasmonics. https://doi.org/10.1007/s11468-022-01631-w
5. Uniyal A, Chauhan B, Pal A, Singh Y (2022) Surface plasmon biosensor based on Bi2Te3 antimonene heterostructure for the detection of cancer cells. Appl Opt 61:3711–3719
6. Patel SK, Argyropoulos C (2015) Plasmonic nanoantennas: enhancing light-matter interactions at the nanoscale. EPJ Appl Metamat 2:1–15
7. Karki B, Uniyal A, Chauhan B, Pal A (2022) Sensitivity enhancement of a graphene, zinc sulfide-based surface plasmon resonance biosensor with an Ag metal configuration in the visible region. J Comput Electron 21:445–452. https://doi.org/10.1007/s10825-022-01854-4
8. Almawgani AH, Daher MG, Taya SA, Olaimat MM, Alhawari AR, Colak I (2022) Detection of blood plasma concentration theoretically using SPR-based biosensor employing black phosphor layers and different metals. Plasmonics
9. Mudgal N, Yupapin P, Ali J et al (2020) BaTiO3-graphene-affinity layer–based surface plasmon resonance (SPR) biosensor for pseudomonas bacterial detection. Plasmonics 15:1221–1229
10. Laref A, Alsagri M, Alay-e-Abbas SM, Laref S, Huang HM, Xiong YC, Yang JT, Khandy SA, Rai DP, Varshney D, Wu X (2020) Electronic structure and optical characteristics of AA stacked bilayer graphene: a first principles calculations. Optik 206:163755
11. Ojaghi S, Golmohammadi S, Soofi H (2021) All-optical graphene-on-silicon slot waveguide modulator based on graphene's Kerr effect. Appl Opt 60:7945–7954
12. Verma R, Gupta BD, Jha R (2011) Sensitivity enhancement of a surface plasmon resonance based biomolecules sensor using graphene and silicon layers. Sens Actuators, B Chem 160(1):623–631
13. Sassi I, Mghaieth R (2020) Infrared thermal source or perfect absorber sensor based on silver 2D grating. Appl Phys A 126:675. https://doi.org/10.1007/s00339-020-03854-2
14. Sassi I, Dhibi A, Oumezzine M (2017) Resonances in reflection, transmission and absorption of 1-D triangular-relief metallic gratings. Indian J Phys 91(2):149–155
15. Eaton SW, Lai M, Gibson NA, Wong AB, Dou L, Ma J, Wang LW, Leone SR, Yang P (2016) Lasing in robust cesium lead halide perovskite nanowires. Proc Natl Acad Sci Vpl 113:1993–1998
16. Dou L, Yang YM, You J, Hong Z, Chang WH, Li G, Yang Y (2014) Solution-processed hybrid perovskite photodetectors with high detectivity. Nat Commun 5:5404
17. Green MA, Ho-Baillie A, Snaith HJ (2014) The emergence of perovskite solar cells. Nat Photonics 8:506–514
18. Wang J, Wang N, Jin Y, Si J, Tan ZK, Du H, Cheng L, Dai X, Bai S, He H, Ye Z, Lai ML, Friend RH, Huang W (2015) Interfacial control toward efcient and low-voltage perovskite lightemitting diodes. Adv Mater 27:2311–2316
19. Leijtens T, Eperon GE, Pathak S, Abate A, Lee MM, Snaith HJ (2013) Overcoming ultraviolet light instability of sensitized TiO2 with meso-superstructured organometal tri-halide perovskite solar cells. Nat Commun 4:2885
20. Hodes G (2013) Applied physics: perovskite-based solar cells. Science 342:317–318
21. Kojima A, Teshima K, Shirai Y, Miyasaka T (2009) Organometal halide perovskites as visible-light sensitizers for photovoltaic cells. J Am Chem Soc 131:6050–6051
22. Kim J, Son H, Cho DJ, Geng B, Regan W, Shi S, Kim K, Zett A, Shen YR, Wang F (2012) Electrical control of optical plasmon resonance with graphene. Nano Lett 12:5598–5602
23. Daher MG, Taya SA, Colak I, Vigneswaran D, Olaimat MM, Patel SK, Ramahi OM, Almawgani AH (2022) Design of a nano-sensor for cancer cell detection based on a ternary photonic crystal with high sensitivity and low detection limit. Chin J Phys 77:1168–1181
24. Rasooly A, Jacobson J (2006) Development of biosensors for cancer clinical testing. Biosens Bioelectron 21(10):1851–1858
25. Hossain B, Paul AK, Islam MA, Rahman MM, Sarkar AK, Abdulrazak LF (2022) A highly sensitive surface plasmon resonance biosensor using SnSe allotrope and heterostructure of BlueP/MoS2 for cancerous cell detection. Optik 252:168506
26. Almawgani AH, Daher MG, Taya SA, Colak I, Patel SK, Ramahi OM (2022) Highly sensitive nano-biosensor based on a binary photonic crystal for cancer cell detection. Opt Quant Electron 54(9):1–19. https://doi.org/10.1007/s11082-022-03978-0
27. Li T, Fan Q, Liu T, Zhu X, Zhao J, Li G (2010) Detection of breast cancer cells specially and accurately by an electrochemical method. Biosensors Bioelectron 25(12):2686–2689
28. Li FR, Li Q, Zhou HX, Qi H, Deng CY (2013) Detection of circulating tumor cells in breast cancer with a refined immunomagnetic nanoparticle enriched assay and nested-RT-PCR, Nanomedicine: Nanotechnology. Biol Med 9(7):1106–1113
29. Hajba L, Guttman A (2014) Circulating tumor-cell detection and capture using microfluidic devices. TrAC, Trends Anal Chem 59(2):9–16
30. Daher MG, Taya SA, Colak I, Patel SK, Olaimat MM, Ramahi O (2022) Surface plasmon resonance biosensor based on graphene layer for the detection of waterborne bacteria. J Biophotonics 15(5):e202200001
31. Almawgani AHM, Daher MG, Taya SA, Mashagbeh M, Colak I (2022) Optical detection of fat concentration in milk using MXene-based surface plasmon resonance structure. Biosensors 12:535. https://doi.org/10.3390/bios12070535
32. Li Y, Gao J, Lu X (2016) An efective antioxidized strategy for Ag based flm-dierlectricmetal plasmonic sensor. 2016 Int Conf Numerical Simulation Optoelectron Devices (NUSOD)
33. Amirjani A, Haghshenas DF (2018) Ag nanostructures as the surface plasmon resonance (SPR)-based sensors: a mechanistic study with an emphasis on heavy metallic ions detection. Sens Actuators B 273:1768–1779
34. Daher MG, Jaroszewicz Z, Zyoud SH, Panda A, Hasane Ahammad SK, Abd-Elnaby M, Eid M, Rashed AN (2022) Design of a novel detector based on photonic crystal nanostructure for ultra-high

performance detection of cells with diabetes. Opt Quant Electron 54(701). https://doi.org/10.1007/s11082-022-04093-w
35. Taya SA, Daher MG (2022) Properties of defect modes of one-dimensional quaternary defective photonic crystal nanostructure. Int J Smart Grid-ijSmartGrid 6(2):29–39
36. Liu C, Liu Q, Xiaotang Hu (2014) SPR phase detection for measuring the thickness of thin metal films. Opt Express 22(7): 7574–7580
37. Prabowo BA, Purwidyantri A, Liu KC (2018) Surface plasmon resonance optical sensor: a review on light source technology. Biosensors 8(3):80
38. Maurya JB, Prajapati YK (2020) Experimental demonstration of DNA hybridization using graphene-based plasmonic sensor chip. IEEE J Lightwave Technol 38(18):5191–5198. https://doi.org/10.1109/JLT.2020.2998138,September15
39. Yao Y, Yi B, Xiao J, Li Z (2007) Surface plasmon resonance biosensors and its application. Proc Int Conf Bioinf Biomed Eng 1043–1046
40. Yeh YL (2008) Real-time measurement of glucose concentration and average refractive index using a laser interferometer. Opt Laser Eng 46:666–670
41. Kuo WK, Tongpakpanang J, Kuo PH, Kuo SF (2019) Implementation and phase detection of dielectric-grating-coupled surface plasmon resonance sensor for backside incident light. Opt Exp 27:3867–3872
42. Singh MK, Verma VK, Pal S, Prajapati YK, Saini JP (2021) Simulation and analysis of SPR-based biosensor with borophene and antimonene layers. Opt Mater 119:111355
43. Shalabney A, Abdulhalim I (2010) Electromagnetic fields distribution in multilayer thin film structures and the origin of sensitivity enhancement in surface plasmon resonance sensors. Sens Actuators A 159(1):24–32
44. Hossain MB, Mehedi IM, Moznuzzaman M, Abdulrazak LF, Hossain MA (2019) High performance refractive index SPR sensor modeling employing graphene tri sheets. Results Phys 15:102719
45. Srivastava A, Verma A, Das R, Prajapati YK (2020) A theoretical approach to improve the performance of SPR biosensor using MXene and black phosphorus. Optik 203:163430
46. Pal S, Prajapati YK, Saini JP (2020) Influence of grapheme'chemical potential on SPR biosensor using ZnO for DNA hybridization. Opt Rev 27:57–64
47. Taya SA, Al-Ashi NE, Ramahi OM, Colak I, Amiri IS (2021) Surface plasmon resonance-based optical sensor using a thin layer of plasma. J Opt Soc Am B 38:2362–2337
48. Karki B, Uniyal A, Pal A, Srivastava V (2022) Advances in surface plasmon resonance-based biosensor technologies for cancer cell detection. Int J Opt. https://doi.org/10.1155/2022/1476254
49. Karki B, Uniyal A, Pal A, Srivastava V (2022) Hemoglobin detection in blood samples using a graphene-based surface plasmon resonance biosensor. Optik 270:169947. https://doi.org/10.1016/j.ijleo.2022.169947

Authors and Affiliations

Malek G. Daher[1,2] · Youssef Trabelsi[3,4] · Naser M. Ahmed[2] · Yogenra Kumar Prajapati[5] · Vishal Sorathiya[6] · Sk Hasane Ahammad[7] · P. Poorna Priya[8] · Osama S. Faragallah[9] · Ahmed Nabih Zaki Rashed[10]

Malek G. Daher
malekjbreel20132017@gmail.com

Youssef Trabelsi
ytrabelsi@kku.edu.sa

Naser M. Ahmed
naser@Uusm.my

Yogenra Kumar Prajapati
yogendrapra@mnnit.ac.in

Vishal Sorathiya
vishal.sorathiya9@gmail.com

Sk Hasane Ahammad
ahammadklu@gmail.com

P. Poorna Priya
hodece@diet.edu.in

Osama S. Faragallah
o.salah@tu.edu.sa

1 Physics Department, Islamic University of Gaza, P.O. Box 108, Gaza, Palestine

2 School of Physics, Universiti Sains Malaysia, 11800 Penang, Malaysia

3 College of Arts and Sciences in Muhail Asir, Physics Department, King Khalid University, Abha, Saudi Arabia

4 University of Tunis El Manar, National Engineering School of Tunis, Photovoltaic and Semiconductor Materials Laboratory, 1002 Tunis, Tunisia

5 Department of Electronics and Communication Engineering, Motilal Nehru National Institute of Technology (MNNIT) Allahabad, Prayagraj, India

6 Faculty of Engineering and Technology, Parul Institute of Engineering and Technology, Parul University, Waghodia Road, Vadodara 391760, Gujarat, India

7 Department of ECE, Koneru Lakshmaiah Education Foundation, Vaddeswaram, India 522302

8 Department of ECE, Dadi Institute of Engineering and Technology, Anakapalle, Visakhapatnam, India

9 Department of Information Technology, College of Computers and Information Technology, Taif University, P.O. Box 11099, Taif 21944, Saudi Arabia

10 Electronics and Electrical Communications Engineering Department, Faculty of Electronic Engineering, Menoufia University, Menouf 32951, Egypt

Terms and Conditions

Springer Nature journal content, brought to you courtesy of Springer Nature Customer Service Center GmbH (“Springer Nature”).
Springer Nature supports a reasonable amount of sharing of research papers by authors, subscribers and authorised users (“Users”), for small-scale personal, non-commercial use provided that all copyright, trade and service marks and other proprietary notices are maintained. By accessing, sharing, receiving or otherwise using the Springer Nature journal content you agree to these terms of use (“Terms”). For these purposes, Springer Nature considers academic use (by researchers and students) to be non-commercial.
These Terms are supplementary and will apply in addition to any applicable website terms and conditions, a relevant site licence or a personal subscription. These Terms will prevail over any conflict or ambiguity with regards to the relevant terms, a site licence or a personal subscription (to the extent of the conflict or ambiguity only). For Creative Commons-licensed articles, the terms of the Creative Commons license used will apply.
We collect and use personal data to provide access to the Springer Nature journal content. We may also use these personal data internally within ResearchGate and Springer Nature and as agreed share it, in an anonymised way, for purposes of tracking, analysis and reporting. We will not otherwise disclose your personal data outside the ResearchGate or the Springer Nature group of companies unless we have your permission as detailed in the Privacy Policy.
While Users may use the Springer Nature journal content for small scale, personal non-commercial use, it is important to note that Users may not:

1. use such content for the purpose of providing other users with access on a regular or large scale basis or as a means to circumvent access control;
2. use such content where to do so would be considered a criminal or statutory offence in any jurisdiction, or gives rise to civil liability, or is otherwise unlawful;
3. falsely or misleadingly imply or suggest endorsement, approval , sponsorship, or association unless explicitly agreed to by Springer Nature in writing;
4. use bots or other automated methods to access the content or redirect messages
5. override any security feature or exclusionary protocol; or
6. share the content in order to create substitute for Springer Nature products or services or a systematic database of Springer Nature journal content.

In line with the restriction against commercial use, Springer Nature does not permit the creation of a product or service that creates revenue, royalties, rent or income from our content or its inclusion as part of a paid for service or for other commercial gain. Springer Nature journal content cannot be used for inter-library loans and librarians may not upload Springer Nature journal content on a large scale into their, or any other, institutional repository.
These terms of use are reviewed regularly and may be amended at any time. Springer Nature is not obligated to publish any information or content on this website and may remove it or features or functionality at our sole discretion, at any time with or without notice. Springer Nature may revoke this licence to you at any time and remove access to any copies of the Springer Nature journal content which have been saved.
To the fullest extent permitted by law, Springer Nature makes no warranties, representations or guarantees to Users, either express or implied with respect to the Springer nature journal content and all parties disclaim and waive any implied warranties or warranties imposed by law, including merchantability or fitness for any particular purpose.
Please note that these rights do not automatically extend to content, data or other material published by Springer Nature that may be licensed from third parties.
If you would like to use or distribute our Springer Nature journal content to a wider audience or on a regular basis or in any other manner not expressly permitted by these Terms, please contact Springer Nature at

onlineservice@springernature.com